ACS APPLIED MATERIALS & INTERFACES

www.acsami.org

Research Article

Carbazole-Terminated Isomeric Hole-Transporting Materials for Perovskite Solar Cells

Kasparas Rakstys,[⊥] Sanghyun Paek,[⊥] Aida Drevilkauskaite, Hiroyuki Kanda, Sarune Daskeviciute, Naoyuki Shibayama, Maryte Daskeviciene, Alytis Gruodis, Egidijus Kamarauskas, Vygintas Jankauskas, Vytautas Getautis,* and Mohammad Khaja Nazeeruddin*

Cite This: *ACS Appl. Mater. Interfaces* 2020, 12, 19710−19717

Read Online

ACCESS | Metrics & More | Article Recommendations | Supporting Information

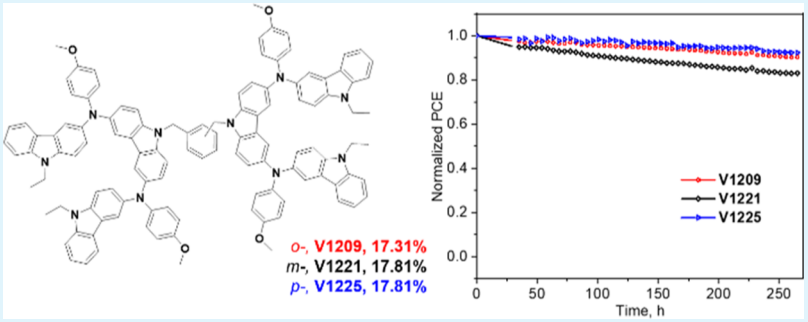

ABSTRACT: A set of novel hole-transporting materials (HTMs) based on π-extension through carbazole units was designed and synthesized via a facile synthetic procedure. The impact of isomeric structural linking on their optical, thermal, electrophysical, and photovoltaic properties was thoroughly investigated by combining the experimental and simulation methods. Ionization energies of HTMs were measured and found to be suitable for a triple-cation perovskite active layer ensuring efficient hole injection. New materials were successfully applied in perovskite solar cells, which yielded a promising efficiency of up to almost 18% under standard 100 mW cm^{-2} global AM1.5G illumination and showed a better stability tendency outperforming that of 2,2′,7,7′-tetrakis-(*N*,*N*-di-*p*-methoxyphenylamine)-9,9′-spirobifluorene. This work provides guidance for the molecular design strategy of effective hole-conducting materials for perovskite photovoltaics and similar electronic devices.

KEYWORDS: *carbazole, hole-transporting material, perovskite, solar cell, isomeric semiconductors*

INTRODUCTION

During the last decade, perovskite solar cells (PSCs) have attracted vast interest in photovoltaic research leading to enormous enhancement in the power conversion efficiency (PCE), currently exceeding 25%.[1−4] The main advantages of PSCs are their simple fabrication methods and relatively inexpensive components that hold great potential for future low-cost energy production enabling the global transition to a low-carbon society.[5,6] The typical PSC consists of a photoactive perovskite material sandwiched between an n-type semiconducting electron transport material and a p-type semiconducting hole transport material (HTM) with selective contacts.[7−10] To further enhance the performance of the PSC device, it is vital to optimize each of the functional layers. Plenty of recent findings have proved that finely modifying the perovskite composition may contribute to improved device performance and stability with the current structure of $Cs_{0.1}((CH_3NH_3)_{0.15}(NH{=}CHNH_3)_{0.85})_{0.9}Pb(I_{0.85}Br_{0.15})$ used as a standard.[11−14] Despite the fact that PSCs have skyrocketed in PCE, there are still several device issues that need to be resolved, especially improving the long-term stability.[15−20] In this context, small organic molecules are particularly appealing because they offer a wide range of structural modifications leading to desired properties and are easy to synthesize, purify, and process.[21−24] Numerous approaches are employed in the development of such HTMs including linear, star-shaped, spiro-centered, or cross-linked structures in order to match the required hydrophobicity, energy levels, and charge carrier mobility.[25−30] To date, 2,2′,7,7′-tetrakis-(*N*,*N*-di-*p*-methoxyphenylamine)-9,9′-spirobifluorene (spiro-OMeTAD) dominates the field and despite its high price (~300 €/g), it is routinely used as a reference standard for research studies providing high efficiency, as it has been well-studied and easily

Received: December 29, 2019
Accepted: April 3, 2020
Published: April 3, 2020

https://dx.doi.org/10.1021/acsami.9b23495
ACS Appl. Mater. Interfaces 2020, 12, 19710−19717

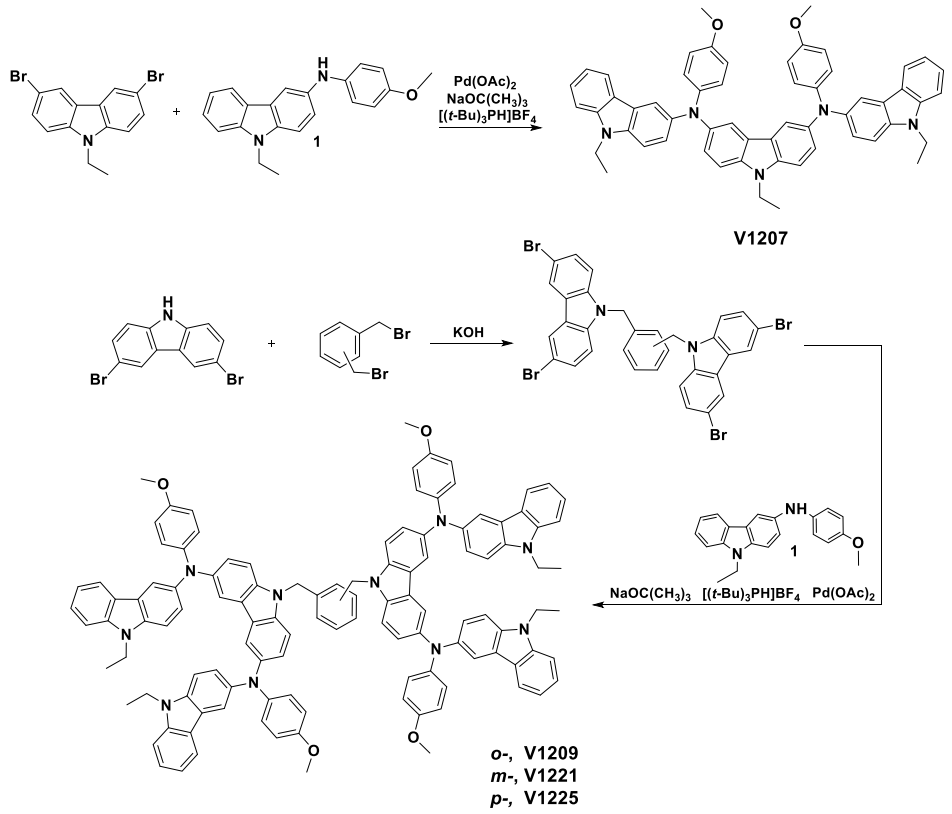

Figure 1. Synthesis routes for target molecules **V1207**, **V1209**, **V1221**, and **V1225**.

available because of its commercialization decades ago.[31] However, the cost-effective industrial potential is hardly probable. Therefore, research interests directed toward the development of novel HTMs have been raised to find an ideal HTM, which would be amenable to scale-up as well as to better reveal the relationship between the molecular structure and the device performance.[32,33] As a result of spiro-OMeTAD success, many research groups have been focused on spiro-type derivatives in order to improve the performance with slight structural modifications including spirobifluorene-based DM,[34] spirofluorenexanthene-based X55[35] and HTM-FX,[36] spirofluorenecyclopentadithiophene-based FDT[37] and dispiro-modified DDOF,[38] G2,[39] and dispiro-OBuTAD.[40]

Carbazole is known to be a promising core unit for molecular design because it can be substituted with a wide range of desired groups, allowing fine-tuning of its linking topologies and optical and electrochemical properties.[41] Various carbazole-structured molecular HTMs have been widely applied in PSCs and showed a comparable photovoltaic performance.[42,43] Dimethoxydiphenylamine-substituted carbazole scaffolds as electron-donating units in the periphery were routinely used to tune the HOMO level of the final semiconducting molecule.[44] This includes star-shaped SGT series;[45,46] benzodithiazole-,[47] bipyridine-,[48] pyrene-based[49] examples and our previous work, where diphenylamine-substituted carbazoles were linked by a nonconjugated simple bismethylenebenzene-binding units using a straightforward synthetic procedure and showed a photovoltaic performance of up to 19%.[50]

In this work, three carbazole-based twin molecules, termed **V1209**, **V1221**, and **V1225**, and a "half" molecule, **V1207**, were designed based on a π-extension through an additional carbazole unit and successfully synthesized. The effects of isomeric linking on various properties of newly synthesized molecules, in comparison to our earlier report, have been systematically investigated. All these carbazole-based HTMs have been successfully applied in PSCs.

RESULTS AND DISCUSSION

General synthetic routes for the preparation of new hole transporters **V1207**, **V1209**, **V1221**, and **V1225** are shown in Figure 1. The "half" molecule **V1207** was obtained by reacting 3,6-dibromo-9-ethyl-9*H*-carbazole and 9-ethyl-*N*-(4-methoxyphenyl)-9*H*-carbazol-3-amine (**1**) under Buchwald−Hartwig amination conditions with the utilization of a palladium catalytic system. In order to obtain twin derivatives, a facile two-step synthetic procedure was employed. First, commercially available isomeric bis(bromomethyl)benzene linkers and 3,6-dibromocarbazole were reacted in a simple click-type reaction, as reported previously.[50,51] Second, tetrabromo-functionalized isomeric central fragments were converted to final products under the same protocol as for **V1207**. Under these conditions, **V1209**, **V1221**, and **V1225** were isolated in high yields of between 72−77%. We note the simplicity of the applied synthetic route requiring no expensive starting materials and tricky purification methods. All detailed synthetic procedures and methods are described in the Supporting Information experimental part with the NMR and MS spectra provided in Figures S10−S17.

Quantum chemical calculations of **V1207**, **V1209**, **V1221**, and **V1225** were performed by means of Gaussian09 software[52] in order to establish the most probable molecular geometry and the corresponding absorption spectrum. Geometry optimization of the ground state structure was provided using the density functional theory method B3LYP

https://dx.doi.org/10.1021/acsami.9b23495
ACS Appl. Mater. Interfaces 2020, 12, 19710−19717

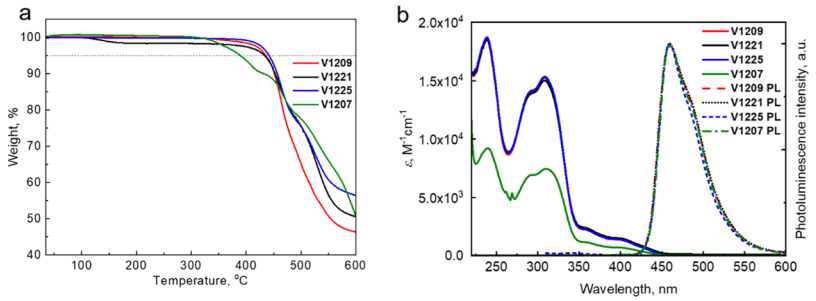

Figure 2. (a) TGA data (heating rate of 10 °C/min, N_2 atmosphere); (b) UV-Vis absorption (solid line) and photoluminescence (dashed line) spectra of V-series HTMs in THF solution (10^{-4} M).

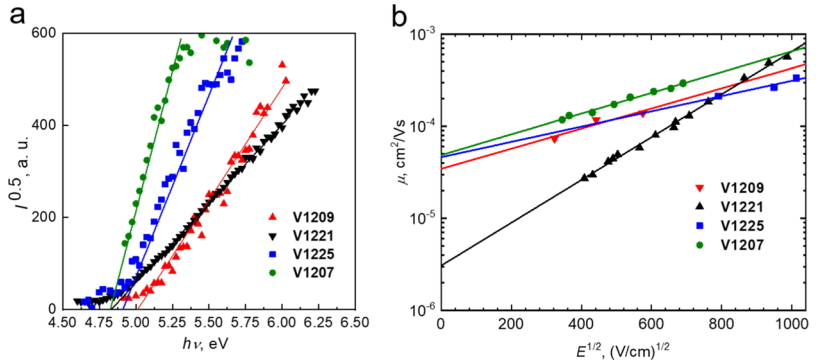

Figure 3. (a) Photoemission in air spectra of HTMs and (b) electric field dependencies of the hole-drift mobility (μ) in charge transport layers of **V1209**, **V1221**, **V1225**, and **V1207**.

and 6-31G basis without polarization functions. Optimized molecular structures (after ground state geometry optimization) in *XY* and *XZ* projections are presented in Figure S1. The electronic absorption spectrum was simulated using a semi-empirical TD method (for singlets only). Environmental effects were not included for all simulations. Table S1 represents the parameters of the four lowest excited states: S_1–S_4. Table S2 represents the impact of molecular orbitals on "spectroscopic" transitions. All transitions between the above-mentioned lowest excited states and the ground state are forbidden (oscillator strength about zero). For **V1207**, the $S_0 \rightarrow S_1$ transition energy is equal to 2.93 eV and the $S_0 \rightarrow S_2$ transition energy is equal to 3.07 eV. For **V1209**, **V1221**, and **V1225** structures, the energies of $S_0 \rightarrow S_1$ and $S_0 \rightarrow S_2$ transitions are approximately equal (2.93 eV, because of degenerate states, corresponding to the $S_0 \rightarrow S_1$ transition of **V1207**), and also the energies of $S_0 \rightarrow S_3$ and $S_0 \rightarrow S_4$ transitions are approximately equal (3.05 eV, corresponding to the $S_0 \rightarrow S_2$ transition of **V1207**). Distributions of the electron density for the HOMO and HOMO−1 as well as the LUMO and LUMO+1 for **V1207**, **V1209**, **V1221**, and **V1225** structures are presented in Figures S2–S5, respectively. CT charge redistribution behavior was established for **V1225** only.

The thermal behavior of HTMs was estimated by thermogravimetric analysis (TGA) (Figure 2a) and differential scanning calorimetry (DSC) (Figure S6) measurements. From TGA, it was found that twin molecules have a similar decomposition temperature (T_{dec}) in the range of 430–440 °C, showing their excellent thermal stability, while **V1207** decomposes at a significantly lower temperature (T_{dec} = 385 °C) because of its smaller aromatic system.[53] The thermal transitions of V-series molecules were determined by DSC. Only the glass transition temperature (T_g) was investigated for all compounds during both heating scans with very small variations (184–192 °C) observed in T_g depending on isomeric central core substitution, while **V1207** has a less stabilized amorphous state with the glass transition detected at 154 °C. In general, DSC traces demonstrate that these HTMs are fully amorphous, which is desired to form homogeneous films upon device fabrication.

The UV-visible absorption and photoluminescence (PL) spectra of the synthesized HTMs are depicted in Figure 2b. All compounds had two major peaks cantered at around 235 and 300 nm. The intense absorption peak at shorter wavelengths correspond to localized π–π^* transitions, while that at longer wavelengths arises from less intensive delocalization from the conjugated scaffold that can be assigned to n–π^* transitions. The change in the central benzene substitution has not influenced the conjugation, therefore the spectra of all twin isomers are identical; however, there is a huge difference in the absorption intensity of the "half" molecule **V1207** arising from the significantly smaller aromatic conjugated system. The PL spectra of all the HTMs were similar and are normalized at the peak value centered at 459 nm, showing that comparably large Stokes shifts of around 150 nm are observed for all molecules meaning significant changes in the geometry of the molecules once excited. The optical gaps (E_g) were calculated from the intersection of absorption and PL spectra and were found to be identical for all the materials at around 2.78 eV.

For better interpretation of energy level alignment of HTMs in perovskite-based devices, the solid-state ionization potential (I_P) of thin films was measured by photoelectron emission spectroscopy in air (PESA) and the experimental data are shown in Figure 3a. **V1209**, **V1221**, **V1225**, and **V1207** were found to have I_P values of 4.93, 4.83, 4.91, and 4.82 eV, respectively, which are very close to that of spiro-OMeTAD

https://dx.doi.org/10.1021/acsami.9b23495
ACS Appl. Mater. Interfaces 2020, 12, 19710–19717

Table 1. Thermal, Optical, and Photophysical Properties of the Synthesized Materials

ID	T_g [°C][a]	T_{dec} [°C][a]	λ_{abs} [nm][b]	λ_{em} [nm][b]	I_p [eV][c]	E_g [eV][d]	μ_0 [cm^2 V^{-1} s^{-1}][e]
V1209	187	432	238, 293, 308	459	4.93	2.78	3.5×10^{-5}
V1221	184	436	238, 294, 308	459	4.83	2.76	3×10^{-6}
V1225	192	441	238, 292, 309	459	4.91	2.78	3×10^{-5}
V1207	154	385	239, 292, 310	459	4.82	2.79	5×10^{-5}

[a]Glass transition (T_g) and decomposition (T_{dec}) temperatures observed from DSC and TGA, respectively (10 °C/min, N_2 atmosphere). [b]Absorption and emission (excitation = $\lambda_{abs\ max}$) spectra measured in THF solution (10^{-4} M). [c]Ionization energies of the films measured using PESA. [d]E_g estimated from the intersection of absorption and emission spectra. [e]Mobility value at zero field strength.

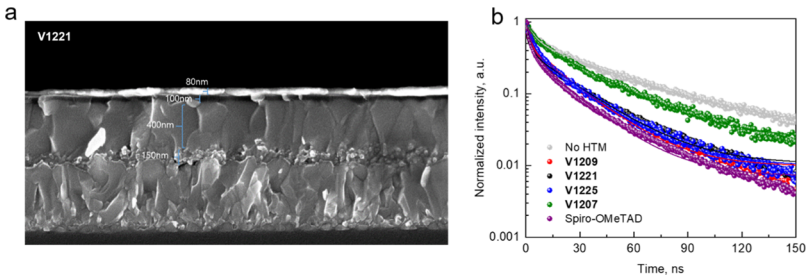

Figure 4. (a) Cross-sectional SEM micrograph of a perovskite device containing **V1221** as the HTM and (b) normalized PL decay in the first 150 ns time window, upon excitation at 480 nm.

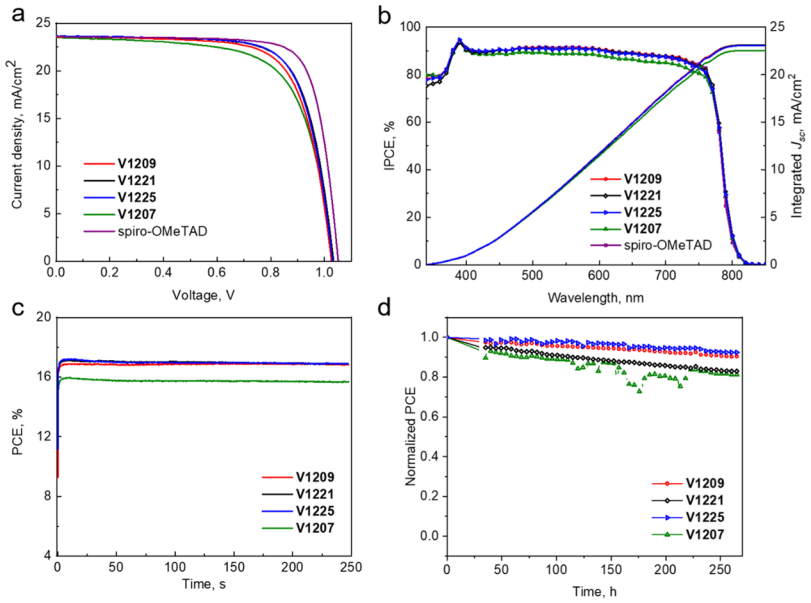

Figure 5. (a) *J*–*V* curves of champion cells employing **V1207**, **V1209**, **V1221**, **V1225,** and spiro-OMeTAD under AM 1.5 illumination; (b) IPCE spectra and integrated currents for the devices with V-series HTMs and spiro-OMeTAD; (c) stabilized PCEs using different HTMs at maximum power point tracking during the 250 s time frame; and (d) stability test of the PSCs under 1 sun illumination.

(5.00 eV) and perfectly align with the valence band energy of the perovskite (~5.5 eV) ensuring efficient hole transfer from the perovskite to the cathode. We next determined the charge mobility of V-series materials using xerographic time of flight technique. The dependence of hole drift mobility on electric field strength is shown in Figure 3b. The zero-field hole drift mobility (μ_0) of **V1209** and **V1225** was determined to be 3.5×10^{-5} and 3×10^{-5} cm^2/V s, respectively, while that of **V1221** was found to be an order of magnitude lower at 3×10^{-6} cm^2/V s, therefore the isomeric substitution change of the central benzene fragment significantly influences the hole drift mobility. A similar trend among differently substituted isomers was previously reported in the literature, showing that *m*-isomers typically have a larger energetic disorder.[54] Interestingly, **V1207** had the highest hole drift mobility value of 5×10^{-5} cm^2/V s, which is slightly below that of spiro-OMeTAD ($\mu_0 = 1.3 \times 10^{-4}$ cm^2/V s).[55] The thermal, optical, and photoelectrical properties of V-series charge-transporting materials are summarized in Table 1.

To prove the function of carbazole-rich HTMs in PSCs, we prepared perovskite cells with mixed triple-cation perovskite as the photoactive light absorber in a mesoporous configuration device stack of fluorine-doped tin oxide (FTO)/compact TiO_2/mesoporous TiO_2 and SnO_2/perovskite/HTM/Au. The solar cell preparation is fully described in the Supporting Information following the method that has been previously optimized for spiro-OMeTAD.[50] We then analyzed the surface of each hole-transporting layer and the cross section of the

https://dx.doi.org/10.1021/acsami.9b23495
ACS Appl. Mater. Interfaces 2020, 12, 19710−19717

following device by high-resolution scanning electron microscopy (SEM). As seen from the top-view SEM images (Figure S7), the perovskite layer was uniformly covered with a smooth HTM film. Figure 4a shows the cross-sectional image of the **V1221**-based PSC, which is made of a 400 nm thick perovskite on top of a 150 nm thick mesoporous TiO_2 layer deposited on FTO glass with precoated compact TiO_2. The device is completed with an HTM layer with a thickness of around 100 nm and gold as a back contact on the top.

Time-resolved PL decay curves (Figure 4b) for HTM-free perovskite along with perovskite/HTM films were recorded using time-correlated single-photon counting (TCSPC) under pulsed excitation at 480 nm. During this procedure, traps were filled, so the decay is associated with the electron−hole recombination processes. The HTM-free perovskite sample shows a long-living component extending out of our time frame. Differently, after the introduction of the hole transport layer the PL decay increases, significant quenching is visible in the first 10 ns. The TCSPC traces were fitted and the obtained time constants are listed in Table S3. Effective quenching of the long-lived species suggests efficient transport of positive charges at the HTM/perovskite interface.

The current density−voltage ($J-V$) curves extracted for PSCs using the hole-transporting layers of **V1207**, **V1209**, **V1221**, and **V1225** under AM1.5G illumination are provided in Figure 5a. Across the V series, the devices using *m*- and *p*-isomers **V1221** and **V1225** as the HTMs showed the highest performance with the identical PCE of 17.81% (16.95% stabilized efficiency, Figure 5c), and the best devices having J_{sc} = 23.6 mA/cm^2, V_{oc} = 1.03 V, and FF = 73, respectively, while the other twin isomer *o*-substituted **V1209** exhibited a slightly lower performance of 17.31%. However, based on the statistical data, **V1221** shows the highest reproducibility among the series. Interestingly, the "half" molecule **V1207** showed a comparable PCE of 16.44%, which is several times higher than the observed trend between the twin and "half" systems in our previous report.[50] One possible explanation could be that the extension of the π-conjugated system with two extra carbazole units improves the charge transport in the film and facilitates the hole extraction. For comparison, we also fabricated a standard device with a spiro-OMeTAD reference, which showed a PCE of 19.34%. The corresponding photovoltaic parameters are summarized in Table 2. In order to reveal the impact of hysteresis on the device performance, $J-V$ curves collected by scanning the applied voltage at 0.1 V s^{-1} from a forward bias to a short circuit and the other way around are reported in Figure S9. $J-V$ curves with the corresponding performance parameters for each HTM showed negligible hysteresis.

Table 2. Performance of the Champion PSC-Based V-Series HTMs Along With Their Average Values Extracted From $J-V$ Curves

ID	V_{oc} [V]	J_{sc} [mA cm^{-2}]	FF	PCE [%]	Avg. PCE [%]
V1207	1.03	23.48	0.68	16.44	15.23
V1209	1.026	23.56	0.716	17.31	16.83
V1221	1.033	23.63	0.73	17.81	17.55
V1225	1.03	23.65	0.731	17.81	17.24
spiro-OMeTAD	1.051	23.62	0.779	19.34	

The incident photon conversion efficiency (IPCE) of the perovskite devices as a function of wavelength with integrated J_{sc} values (Figure 5b) shows that the devices with new HTMs convert around 90% of incoming photons in the whole wavelength range from 400 to 800 nm. The integrated photocurrents calculated from the overlap integral of the IPCE spectra are consistent with those obtained from the experimental $J-V$ measurements and show similar trends. We conducted the stability test at a maximum power point (MMP) under AM 1.5G illumination of 250 s, as shown in Figure 5c. All new HTM devices exhibit less than 5% PCE reduction, while the devices maintain very stable output. Finally, the stability assessment of the devices containing novel HTMs was carried out. In Figure 5d, the maximum power point tracking of each HTM-based perovskite devices is shown. During the testing, unsealed devices were kept in an argon environment under a constant illumination of 100 mW cm^{-2}. The devices were maintained at the maximum power point during aging and the $J-V$ curves were recorded automatically every 3 h. The testing revealed that all HTMs show similar stability, where **V1207** and **V1221** have the lowest resistance to light soaking and lost almost 20% of the initial efficiency after 250 h, while **V1209** and **V1225** showed a better tendency and only a slight decrease in the device efficiency is observed during the testing period. Importantly, all newly developed HTMs show better resistance to light soaking and outperform spiro-OMeTAD, as shown in Figure S18.

CONCLUSIONS

In summary, we present the synthesis of a series of novel carbazole-terminated hole-transporting materials and a systematic study of the impact of an isomeric-linking unit on thermal, optical, photophysical, and photovoltaic properties. Twin molecules **V1209**, **V1221**, and **V1225** exhibit excellent thermal stability up to 440 °C combined with suitable ionization energies that properly align with the valence band of the perovskite absorber. Additionally, the hole drift mobility values of isomers reached 10^{-5} cm^2/Vs order of magnitude, which is comparable with spiro-OMeTAD. The most efficient perovskite devices contained double-armed HTMs **V1221** and **V1225** reaching a PCE of 17.81%; however, **V1221** shows slightly higher reproducibility based on the statistical data. Importantly, all newly developed HTMs show better resistance to light soaking and outperform spiro-OMeTAD, and therefore hold a great prospect for practical wide-scale applications in optoelectronic devices.

ASSOCIATED CONTENT

Supporting Information

The Supporting Information is available free of charge at https://pubs.acs.org/doi/10.1021/acsami.9b23495.

Experimental part, optimized molecular structures and their *XY* projections, additional figures and tables (measurements of DSC, SEM, hysteresis, NMR and MS spectra, etc.) (PDF)

AUTHOR INFORMATION

Corresponding Authors

Vytautas Getautis − *Department of Organic Chemistry, Kaunas University of Technology, Kaunas 50254, Lithuania;* orcid.org/0000-0001-7695-4677; Email: vytautas.getautis@ktu.lt

https://dx.doi.org/10.1021/acsami.9b23495
ACS Appl. Mater. Interfaces 2020, 12, 19710−19717

Mohammad Khaja Nazeeruddin − *Group for Molecular Engineering of Functional Material, Institute of Chemical Sciences and Engineering, École Polytechnique Fédérale de Lausanne, Sion CH-1951, Switzerland;* orcid.org/0000-0001-5955-4786; Email: mdkhaja.nazeeruddin@epfl.ch

Authors

Kasparas Rakstys − *Department of Organic Chemistry, Kaunas University of Technology, Kaunas 50254, Lithuania*

Sanghyun Paek − *Group for Molecular Engineering of Functional Material, Institute of Chemical Sciences and Engineering, École Polytechnique Fédérale de Lausanne, Sion CH-1951, Switzerland; Department of Chemistry and Energy Engineering, Sangmyung University, Seoul 03016, Republic of Korea;* orcid.org/0000-0002-2671-2909

Aida Drevilkauskaite − *Department of Organic Chemistry, Kaunas University of Technology, Kaunas 50254, Lithuania*

Hiroyuki Kanda − *Group for Molecular Engineering of Functional Material, Institute of Chemical Sciences and Engineering, École Polytechnique Fédérale de Lausanne, Sion CH-1951, Switzerland*

Sarune Daskeviciute − *Department of Organic Chemistry, Kaunas University of Technology, Kaunas 50254, Lithuania*

Naoyuki Shibayama − *Department of General Systems Studies, Graduate School of Arts and Sciences, The University of Tokyo, Tokyo 153-8902, Japan;* orcid.org/0000-0003-2182-049X

Maryte Daskeviciene − *Department of Organic Chemistry, Kaunas University of Technology, Kaunas 50254, Lithuania*

Alytis Gruodis − *Institute of Chemical Physics Vilnius University, Vilnius 10257, Lithuania*

Egidijus Kamarauskas − *Institute of Chemical Physics Vilnius University, Vilnius 10257, Lithuania*

Vygintas Jankauskas − *Institute of Chemical Physics Vilnius University, Vilnius 10257, Lithuania*

Complete contact information is available at: https://pubs.acs.org/10.1021/acsami.9b23495

Author Contributions

[⊥]K.R. and P.S. contributed equally to this work.

Notes

The authors declare no competing financial interest.

■ ACKNOWLEDGMENTS

The authors acknowledge funding from the Innosuisse project CTI 25590.1 PFNM-NM, Solaronix, Aubonne, Switzerland. The research leading to these results received funding from the European Union's Horizon 2020 research and innovation programme under grant agreement no. 763977 of the PerTPV project. Computations were performed on resources at the High Performance Computing Center "HPC Sauletekis" (Faculty of Physics, Vilnius University). K.R. acknowledges the funding received from MJJ Foundation.

■ REFERENCES

(1) Kojima, A.; Teshima, K.; Shirai, Y.; Miyasaka, T. Organometal Halide Perovskites as Visible-Light Sensitizers for Photovoltaic Cells. *J. Am. Chem. Soc.* **2009**, *131*, 6050−6051.

(2) Lee, M. M.; Teuscher, J.; Miyasaka, T.; Murakami, T. N.; Snaith, H. J. Efficient Hybrid Solar Cells Based on Meso-Superstructured Organometal Halide Perovskites. *Science* **2012**, *338*, 643−647.

(3) Kim, H.-S.; Lee, C.-R.; Im, J.-H.; Lee, K.-B.; Moehl, T.; Marchioro, A.; Moon, S.-J.; Humphry-Baker, R.; Yum, J.-H.; Moser, J. E.; Grätzel, M.; Park, N.-G. Lead Iodide Perovskite Sensitized All-Solid-State Submicron Thin Film Mesoscopic Solar Cell with Efficiency Exceeding 9%. *Sci. Rep.* **2012**, *2*, 591.

(4) Best Research-Cell Efficiency Chart|Photovoltaic Research| NREL https://www.nrel.gov/pv/cell-efficiency.html (accessed Dec 20, 2019).

(5) Burschka, J.; Pellet, N.; Moon, S.-J.; Humphry-Baker, R.; Gao, P.; Nazeeruddin, M. K.; Grätzel, M. Sequential Deposition as a Route to High-Performance Perovskite-Sensitized Solar Cells. *Nature* **2013**, *499*, 316−319.

(6) Pellet, N.; Gao, P.; Gregori, G.; Yang, T.-Y.; Nazeeruddin, M. K.; Maier, J.; Grätzel, M. Mixed-Organic-Cation Perovskite Photovoltaics for Enhanced Solar-Light Harvesting. *Angew. Chem., Int. Ed.* **2014**, *53*, 3151−3157.

(7) Yusoff, A. R. B. M.; Nazeeruddin, M. K. Organohalide Lead Perovskites for Photovoltaic Applications. *J. Phys. Chem. Lett.* **2016**, *7*, 851−866.

(8) Park, N.-G. Perovskite Solar Cells: An Emerging Photovoltaic Technology. *Mater. Today* **2015**, *18*, 65−72.

(9) Green, M. A.; Ho-Baillie, A.; Snaith, H. J. The Emergence of Perovskite Solar Cells. *Nat. Photonics* **2014**, *8*, 506−514.

(10) Rakstys, K.; Stephen, M.; Saghaei, J.; Jin, H.; Gao, M.; Zhang, G.; Hutchinson, K.; Chesman, A.; Burn, P. L.; Gentle, I.; Shaw, P. E. Precursor Route Poly(1,4-Phenylenevinylene)-Based Interlayers for Perovskite Solar Cells. *ACS Appl. Energy Mater.* **2020**, *3*, 889−899.

(11) Saliba, M.; Matsui, T.; Seo, J.-Y.; Domanski, K.; Correa-Baena, J.-P.; Nazeeruddin, M. K.; Zakeeruddin, S. M.; Tress, W.; Abate, A.; Hagfeldt, A.; Grätzel, M. Cesium-Containing Triple Cation Perovskite Solar Cells: Improved Stability, Reproducibility and High Efficiency. *Energy Environ. Sci.* **2016**, *9*, 1989−1997.

(12) Saliba, M.; Matsui, T.; Domanski, K.; Seo, J.-Y.; Ummadisingu, A.; Zakeeruddin, S. M.; Correa-Baena, J.-P.; Tress, W. R.; Abate, A.; Hagfeldt, A.; Gratzel, M. Incorporation of Rubidium Cations into Perovskite Solar Cells Improves Photovoltaic Performance. *Science* **2016**, *354*, 206−209.

(13) Jodlowski, A. D.; Roldán-Carmona, C.; Grancini, G.; Salado, M.; Ralaiarisoa, M.; Ahmad, S.; Koch, N.; Camacho, L.; De Miguel, G.; Nazeeruddin, M. K. Large Guanidinium Cation Mixed with Methylammonium in Lead Iodide Perovskites for 19% Efficient Solar Cells. *Nat. Energy* **2017**, *2*, 972−979.

(14) Zheng, X.; Chen, B.; Dai, J.; Fang, Y.; Bai, Y.; Lin, Y.; Wei, H.; Zeng, X. C.; Huang, J. Defect Passivation in Hybrid Perovskite Solar Cells Using Quaternary Ammonium Halide Anions and Cations. *Nat. Energy* **2017**, *2*, 17102.

(15) Divitini, G.; Cacovich, S.; Matteocci, F.; Cinà, L.; Di Carlo, A.; Ducati, C. In Situ Observation of Heat-Induced Degradation of Perovskite Solar Cells. *Nat. Energy* **2016**, *1*, 15012.

(16) Han, Y.; Meyer, S.; Dkhissi, Y.; Weber, K.; Pringle, J. M.; Bach, U.; Spiccia, L.; Cheng, Y.-B. Degradation Observations of Encapsulated Planar $CH_3NH_3PbI_3$ Perovskite Solar Cells at High Temperatures and Humidity. *J. Mater. Chem. A* **2015**, *3*, 8139−8147.

(17) Aristidou, N.; Sanchez-Molina, I.; Chotchuangchutchaval, T.; Brown, M.; Martinez, L.; Rath, T.; Haque, S. A. The Role of Oxygen in the Degradation of Methylammonium Lead Trihalide Perovskite Photoactive Layers. *Angew. Chem., Int. Ed.* **2015**, *54*, 8208−8212.

(18) Leijtens, T.; Eperon, G. E.; Pathak, S.; Abate, A.; Lee, M. M.; Snaith, H. J. Overcoming Ultraviolet Light Instability of Sensitized TiO2 with Meso-Superstructured Organometal Tri-Halide Perovskite Solar Cells. *Nat. Commun.* **2013**, *4*, 2885.

(19) Ma, S.; Qiao, W.; Cheng, T.; Zhang, B.; Yao, J.; Alsaedi, A.; Hayat, T.; Ding, Y.; Tan, Z. a.; Dai, S. Optical-Electrical-Chemical Engineering of PEDOT:PSS by Incorporation of Hydrophobic Nafion for Efficient and Stable Perovskite Solar Cells. *ACS Appl. Mater. Interfaces* **2018**, *10*, 3902−3911.

(20) Yang, Y.; Peng, H.; Liu, C.; Arain, Z.; Ding, Y.; Ma, S.; Liu, X.; Hayat, T.; Alsaedi, A.; Dai, S. Bi-Functional Additive Engineering for High-Performance Perovskite Solar Cells with Reduced Trap Density. *J. Mater. Chem. A* **2019**, *7*, 6450−6458.

(21) Lian, X.; Zhao, Z.; Cheng, D. Recent Progress on Triphenylamine Materials: Synthesis, Properties, and Applications. *Mol. Cryst. Liq. Cryst.* **2017**, *648*, 223−235.
(22) Agarwala, P.; Kabra, D. A Review on Triphenylamine (TPA) Based Organic Hole Transport Materials (HTMs) for Dye Sensitized Solar Cells (DSSCs) and Perovskite Solar Cells (PSCs): Evolution and Molecular Engineering. *J. Mater. Chem. A* **2017**, *5*, 1348−1373.
(23) Myers, J. D.; Xue, J. Organic Semiconductors and Their Applications in Photovoltaic Devices. *Polym. Rev.* **2012**, *52*, 1−37.
(24) Saragi, T. P. I.; Spehr, T.; Siebert, A.; Fuhrmann-Lieker, T.; Salbeck, J. Spiro Compounds for Organic Optoelectronics. *Chem. Rev.* **2007**, *107*, 1011−1065.
(25) Swetha, T.; Singh, S. P. Perovskite Solar Cells Based on Small Molecule Hole Transporting Materials. *J. Mater. Chem. A* **2015**, *3*, 18329−18344.
(26) Urieta-Mora, J.; García-Benito, I.; Molina-Ontoria, A.; Martín, N. Hole Transporting Materials for Perovskite Solar Cells: A Chemical Approach. *Chem. Soc. Rev.* **2018**, *47*, 8541−8571.
(27) Yan, W.; Ye, S.; Li, Y.; Sun, W.; Rao, H.; Liu, Z.; Bian, Z.; Huang, C. Hole-Transporting Materials in Inverted Planar Perovskite Solar Cells. *Adv. Energy Mater.* **2016**, *6*, 1600474.
(28) Teh, C. H.; Daik, R.; Lim, E. L.; Yap, C. C.; Ibrahim, M. A.; Ludin, N. A.; Sopian, K.; Mat Teridi, M. A. A Review of Organic Small Molecule-Based Hole-Transporting Materials for Meso-Structured Organic−Inorganic Perovskite Solar Cells. *J. Mater. Chem. A* **2016**, *4*, 15788−15822.
(29) Rakstys, K.; Igci, C.; Nazeeruddin, M. K. Efficiency vs. Stability: Dopant-Free Hole Transporting Materials towards Stabilized Perovskite Solar Cells. *Chem. Sci.* **2019**, *10*, 6748−6769.
(30) Bakr, Z. H.; Wali, Q.; Fakharuddin, A.; Schmidt-Mende, L.; Brown, T. M.; Jose, R. Advances in Hole Transport Materials Engineering for Stable and Efficient Perovskite Solar Cells. *Nano Energy* **2017**, *34*, 271−305.
(31) Bach, U.; Lupo, D.; Comte, P.; Moser, J. E.; Weissörtel, F.; Salbeck, J.; Spreitzer, H.; Grätzel, M. Solid-State Dye-Sensitized Mesoporous TiO2 Solar Cells with High Photon-to-Electron Conversion Efficiencies. *Nature* **1998**, *395*, 583−585.
(32) Ma, X. J.; Zhu, X. D.; Wang, K. L.; Igbari, F.; Yuan, Y.; Zhang, Y.; Gao, C. H.; Jiang, Z. Q.; Wang, Z. K.; Liao, L. S. Planar Starburst Hole-Transporting Materials for Highly Efficient Perovskite Solar Cells. *Nano Energy* **2019**, *63*, 103865.
(33) Zhu, X. D.; Ma, X. J.; Wang, Y. K.; Li, Y.; Gao, C. H.; Wang, Z. K.; Jiang, Z. Q.; Liao, L. S. Hole-Transporting Materials Incorporating Carbazole into Spiro-Core for Highly Efficient Perovskite Solar Cells. *Adv. Funct. Mater.* **2019**, *29*, 1807094.
(34) Jeon, N. J.; Na, H.; Jung, E. H.; Yang, T. Y.; Lee, Y. G.; Kim, G.; Shin, H. W.; Il Seok, S.; Lee, J.; Seo, J. A Fluorene-Terminated Hole-Transporting Material for Highly Efficient and Stable Perovskite Solar Cells. *Nat. Energy* **2018**, *3*, 1−8.
(35) Xu, B.; Zhang, J.; Hua, Y.; Liu, P.; Wang, L.; Ruan, C.; Li, Y.; Boschloo, G.; Johansson, E. M. J.; Kloo, L.; Hagfeldt, A.; Jen, A. K. Y.; Sun, L. Tailor-Making Low-Cost Spiro[Fluorene-9,9′-Xanthene]-Based 3D Oligomers for Perovskite Solar Cells. *Chem* **2017**, *2*, 676−687.
(36) Chiykowski, V. A.; Cao, Y.; Tan, H.; Tabor, D. P.; Sargent, E. H.; Aspuru-Guzik, A.; Berlinguette, C. P. Precise Control of Thermal and Redox Properties of Organic Hole-Transport Materials. *Angew. Chem., Int. Ed.* **2018**, *57*, 15529−15533.
(37) Saliba, M.; Orlandi, S.; Matsui, T.; Aghazada, S.; Cavazzini, M.; Correa-Baena, J.-P.; Gao, P.; Scopelliti, R.; Mosconi, E.; Dahmen, K.-H.; De Angelis, F.; Abate, A.; Hagfeldt, A.; Pozzi, G.; Graetzel, M.; Nazeeruddin, M. K. A Molecularly Engineered Hole-Transporting Material for Efficient Perovskite Solar Cells. *Nat. Energy* **2016**, *1*, 15017.
(38) Rakstys, K.; Paek, S.; Sohail, M.; Gao, P.; Cho, K. T.; Gratia, P.; Lee, Y.; Dahmen, K. H.; Nazeeruddin, M. K. A Highly Hindered Bithiophene-Functionalized Dispiro-Oxepine Derivative as an Efficient Hole Transporting Material for Perovskite Solar Cells. *J. Mater. Chem. A* **2016**, *4*, 18259−18264.
(39) Gao, K.; Xu, B.; Hong, C.; Shi, X.; Liu, H.; Li, X.; Xie, L.; Jen, A. K.-Y. Di-Spiro-Based Hole-Transporting Materials for Highly Efficient Perovskite Solar Cells. *Adv. Energy Mater.* **2018**, *8*, 1800809.
(40) Yu, W.; Zhang, J.; Wang, X.; Liu, X.; Tu, D.; Zhang, J.; Guo, X.; Li, C. A Dispiro-Type Fluorene-Indenofluorene-Centered Hole Transporting Material for Efficient Planar Perovskite Solar Cells. *Sol. RRL* **2018**, *2*, 1800048.
(41) Jiang, H.; Sun, J.; Zhang, J. A Review on Synthesis of Carbazole-Based Chromophores as Organic Light-Emitting Materials. *Curr. Org. Chem.* **2012**, *16*, 2014−2025.
(42) Chen, Z.; Li, H.; Zheng, X.; Zhang, Q.; Li, Z.; Hao, Y.; Fang, G. Low-Cost Carbazole-Based Hole-Transport Material for Highly Efficient Perovskite Solar Cells. *ChemSusChem* **2017**, *10*, 3111−3117.
(43) Liu, X.; Ding, X.; Ren, Y.; Yang, Y.; Ding, Y.; Liu, X.; Alsaedi, A.; Hayat, T.; Yao, J.; Dai, S. A Star-Shaped Carbazole-Based Hole-Transporting Material with Triphenylamine Side Arms for Perovskite Solar Cells. *J. Mater. Chem. C* **2018**, *6*, 12912−12918.
(44) Yu, W.; Yang, Q.; Zhang, J.; Tu, D.; Wang, X.; Liu, X.; Li, G.; Guo, X.; Li, C. Simple Is Best: A p-Phenylene Bridging Methoxydiphenylamine-Substituted Carbazole Hole Transporter for High-Performance Perovskite Solar Cells. *ACS Appl. Mater. Interfaces* **2019**, *11*, 30065−30071.
(45) Kang, M. S.; Sung, S. D.; Choi, I. T.; Kim, H.; Hong, M.; Kim, J.; Lee, W. I.; Kim, H. K. Novel Carbazole-Based Hole-Transporting Materials with Star-Shaped Chemical Structures for Perovskite-Sensitized Solar Cells. *ACS Appl. Mater. Interfaces* **2015**, *7*, 22213−22217.
(46) Lu, C.; Choi, I. T.; Kim, J.; Kim, H. K. Simple Synthesis and Molecular Engineering of Low-Cost and Star-Shaped Carbazole-Based Hole Transporting Materials for Highly Efficient Perovskite Solar Cells. *J. Mater. Chem. A* **2017**, *5*, 20263−20276.
(47) Wu, F.; Ji, Y.; Zhong, C.; Liu, Y.; Tan, L.; Zhu, L. Fluorine-Substituted Benzothiadiazole-Based Hole Transport Materials for Highly Efficient Planar Perovskite Solar Cells with a FF Exceeding 80%. *Chem. Commun.* **2017**, *53*, 8719−8722.
(48) Wu, F.; Shan, Y.; Qiao, J.; Zhong, C.; Wang, R.; Song, Q.; Zhu, L. Replacement of Biphenyl by Bipyridine Enabling Powerful Hole Transport Materials for Efficient Perovskite Solar Cells. *ChemSusChem* **2017**, *10*, 3833−3838.
(49) Li, D.; Shao, J.-Y.; Li, Y.; Li, Y.; Deng, L.-Y.; Zhong, Y.-W.; Meng, Q. New Hole Transporting Materials for Planar Perovskite Solar Cells. *Chem. Commun.* **2018**, *54*, 1651−1654.
(50) Magomedov, A.; Paek, S.; Gratia, P.; Kasparavicius, E.; Daskeviciene, M.; Kamarauskas, E.; Gruodis, A.; Jankauskas, V.; Kantminiene, K.; Cho, K. T.; Rakstys, K.; Malinauskas, T.; Getautis, V.; Nazeeruddin, M. K. Diphenylamine-Substituted Carbazole-Based Hole Transporting Materials for Perovskite Solar Cells: Influence of Isomeric Derivatives. *Adv. Funct. Mater.* **2018**, *28*, 1704351.
(51) Gratia, P.; Magomedov, A.; Malinauskas, T.; Daskeviciene, M.; Abate, A.; Ahmad, S.; Grätzel, M.; Getautis, V.; Nazeeruddin, M. K. A Methoxydiphenylamine-Substituted Carbazole Twin Derivative: An Efficient Hole-Transporting Material for Perovskite Solar Cells. *Angew. Chem., Int. Ed.* **2015**, *54*, 11409−11413.
(52) Frisch, M. J.; Trucks, G. W.; Schlegel, H. B.; Scuseria, G. E.; Robb, M. A.; Cheeseman, J. R.; Scalmani, G.; Barone, V.; Mennucci, B.; Petersson, G. A.; Nakatsuji, H.; Caricato, M.; Li, X.; Hratchian, H. P.; Izmaylov, A. F.; Bloino, J.; Zheng, G.; Sonnenberg, J. L.; Hada, M.; Ehara, M.; Toyota, K.; Fukuda, R.; Hasegawa, J.; Ishida, M.; Nakajima, T.; Honda, Y.; Kitao, O.; Nakai, H.; Vreven, T.; Montgomery, J. A.; Peralta, J. E.; Ogliaro, F.; Bearpark, M.; Heyd, J. J.; Brothers, E.; Kudin, K. N.; Staroverov, V. N.; Kobayashi, R.; Normand, J.; Raghavachari, K.; Rendell, A.; Burant, J. C.; Iyengar, S. S.; Tomasi, J.; Cossi, M.; Rega, N.; Millam, J. M.; Klene, M.; Knox, J. E.; Cross, J. B.; Bakken, V.; Adamo, C.; Jaramillo, J.; Gomperts, R.; Stratmann, R. E.; Yazyev, O.; Austin, A. J.; Cammi, R.; Pomelli, C.; Ochterski, J. W.; Martin, R. L.; Morokuma, K.; Zakrzewski, V. G.; Voth, G. A.; Salvador, P.; Dannenberg, J. J.; Dapprich, S.; Daniels, A. D.; Farkas, Ö.; Foresman, J. B.; Ortiz, J. V.; Cioslowski, J.; Fox, D. J.

https://dx.doi.org/10.1021/acsami.9b23495
ACS Appl. Mater. Interfaces 2020, 12, 19710−19717

Gaussian 09 Citation | Gaussian.com. http://gaussian.com/g09citation/ (accessed Dec 20, 2019).
(53) Rakstys, K.; Abate, A.; Dar, M. I.; Gao, P.; Jankauskas, V.; Jacopin, G.; Kamarauskas, E.; Kazim, S.; Ahmad, S.; Grätzel, M.; Nazeeruddin, M. K.; Gratzel, M.; Nazeeruddin, M. K. Triazatruxene-Based Hole Transporting Materials for Highly Efficient Perovskite Solar Cells. *J. Am. Chem. Soc.* **2015**, *137*, 16172−16178.
(54) Shirota, Y. Organic Materials for Electronic and Optoelectronic Devices. *J. Mater. Chem.* **2000**, *10*, 1−25.
(55) Rakstys, K.; Paek, S.; Grancini, G.; Gao, P.; Jankauskas, V.; Asiri, A. M.; Nazeeruddin, M. K. Low-Cost Perovskite Solar Cells Employing Dimethoxydiphenylamine-Substituted Bistricyclic Aromatic Enes as Hole Transport Materials. *ChemSusChem* **2017**, *10*, 3825−3832.

https://dx.doi.org/10.1021/acsami.9b23495
ACS Appl. Mater. Interfaces 2020, 12, 19710−19717